

An Efficient Algorithm for Non-Negative Matrix Factorization with Random Projections

Gabriele Torre and Michael Graber

University of Applied Science and Art Northwestern Switzerland (FHNW)

Contact: `firstname.lastname@fhnw.ch`

December 7, 2017

Abstract

Non-negative matrix factorization (NMF) is one of the most popular decomposition techniques for multivariate data. NMF is a core method for many machine-learning related computational problems, such as data compression, feature extraction, word embedding, recommender systems etc. In practice, however, its application is challenging for large datasets. The efficiency of NMF is constrained by long data loading times, by large memory requirements and by limited parallelization capabilities. Here we present a novel and efficient compressed NMF algorithm. Our algorithm applies a random compression scheme to drastically reduce the dimensionality of the problem, preserving well the pairwise distances between data points and inherently limiting the memory and communication load. Our algorithm supersedes existing methods in speed. Nonetheless, it matches the best non-compressed algorithms in reconstruction precision.

1 Introduction

Matrix factorizations constitute a fundamental pillar of numerous machine learning methods. Essentially, matrix factorizations allow the approximate decomposition of a multi-dimensional dataset into a linear combination of a limited set of components. The set of machine learning problems that can be tackled by the use of matrix factorization are quite different in nature and span from dimensionality reduction over blind source separation to the prediction of ratings in collaborative filtering.

Principal Component Analysis (PCA) can be viewed as the most prominent matrix factorization method. It allows to find mutually orthogonal, i.e. uncorrelated, basis vectors along whose directions a given dataset shows decreasing variance. By approximating the data points as linear combinations of a limited number of such orthonormal basis vectors, PCA allows to capture as much variance of the data as possible with a limited number of components. In this way, PCA can serve as an efficient *data compression* technique.

Independent Component Analysis (ICA) allows to find basis vectors that are statistically independent.

This represents a stronger constraint on the basis vectors than being uncorrelated. However, for certain applications this is desirable: ICA is well suited for the task of *blind source separation*, where different signal sources can be assumed to be statistically independent [10].

According to the conditions of orthogonality and independence imposed by PCA and ICA respectively, both of them find components that are mutually constrained. The support of the resulting component variables, however, is unconstrained, and often lead to basis vectors that cannot be easily interpreted. A natural property of many datasets is to have variables with non-negative support. For example, count-based measurements constitute a wide-ranging set of examples for non-negative datasets, including images based on photon counts, text document representations based on word counts or customer-product associations based on click or purchase counts. Moreover, radiation spectra or network distance measurements represent additional prominent non-negative dataset types.

Non-negative Matrix Factorization (NMF) allows for the decomposition of non-negative datasets into two non-negative matrix factors. Unlike PCA or ICA, NMF does not find components that are mutually orthogonal or independent. It computes an approximation of the original dataset in terms of additive linear combination of intrinsic non-negative features. This often facilitates the discovery of naturally interpretable or even physically meaningful data components where no further mutual geometric restrictions are necessary.

For this reason NMF has attracted interest during the last decade not only in the fields of machine learning and data mining but also in application domains, e.g. in Astronomy [1], Cosmology [26], Neuroscience [18], Recommender Systems [27], and Document Clustering [21].

Despite its popularity, the application of standard NMF algorithms on large, high-dimensional data is restricted by their memory requirements. Standard NMF algorithms typically store the entire dataset in memory throughout the whole computational process. For this reason, the application of NMF methods on large datasets is often impractical.

To address these issues [25] and [11] recently introduced new NMF methods based on distributed and parallel computation concepts. Furthermore, [24] and [22] showed that by using Semi-NMF methods [8] in combination with *Random Projection* [23] the dimensionality of the problem can be drastically reduced and the underlying tasks solved much more efficiently. It was proven that this approach is computationally more efficient and requires less memory when being compared to standard NMF algorithms [15]. Moreover, *Random Projections* only marginally affect the quality of the NMF final results [22].

In this paper we propose to incorporate a data compression scheme based on *Random Projection* in the family of Hierarchical Alternating Least Square (HALS) NMF methods. HALS and FastHALS [4, 6] are currently the fastest existing NMF algorithms. We will give a theoretical derivation of the methods and provide an empirical evaluation of their accuracy and numerical performances.

The structure of the paper is the following: In Section 2 we provide an introduction to the decomposition problem for non-negative datasets together with some of the most popular NMF methods. In

Section 3 we introduce the Random Projection technique as a data compression method. The detailed derivation of our algorithm is provided in Section 4. In Section 5 we present a set of experimental results obtained by means of the new NMF method and Section 6 is devoted to our final discussions and considerations about the provided results.

2 Model and Problem Statements

For a given non-negative matrix $\mathbf{X} \in \mathbb{R}_+^{d \times n}$ composed of d datapoints of dimensionality n , NMF seeks to identify the two non-negative factors $\mathbf{A} \in \mathbb{R}_+^{d \times k}$ and $\mathbf{B} \in \mathbb{R}_+^{n \times k}$, that provide a low-rank approximation of the form:

$$\mathbf{X} \sim \mathbf{A}\mathbf{B}^T, \quad (1)$$

where $k \ll \min(d, n)$ represents the desired number of components. We introduce the cost function $J(\mathbf{A}, \mathbf{B} | \mathbf{X})$ as the squared Euclidean distance (*Frobenius norm*) between the data \mathbf{X} and the computed approximation $\mathbf{A}\mathbf{B}^T$. Starting from $J(\mathbf{A}, \mathbf{B} | \mathbf{X})$, the global optimization problem of finding \mathbf{A} and \mathbf{B} given \mathbf{X} can be expressed as:

$$\underset{\mathbf{A}, \mathbf{A} \geq 0; \mathbf{B}, \mathbf{B} \geq 0}{\operatorname{argmin}} J(\mathbf{A}, \mathbf{B} | \mathbf{X}) = \frac{1}{2} \|\mathbf{X} - \mathbf{A}\mathbf{B}^T\|_F^2. \quad (2)$$

Considering both \mathbf{A} and \mathbf{B} as variables of equation (2), it has been proven that $J(\mathbf{A}, \mathbf{B} | \mathbf{X})$ is a non-convex function [16]. However, we can find two convex sub-problems if we consider \mathbf{A} and \mathbf{B} individually. Accordingly, a *block-coordinate descent* approach [16] allows to compute values for \mathbf{A} and \mathbf{B} that correspond to a *local* minimum of $J(\mathbf{A}, \mathbf{B} | \mathbf{X})$.

2.1 Block Coordinate Descent Methods

Generally, the iterative scheme adopted by block-coordinate descent algorithms is to cyclically update *blocks* of variables only, while keeping the remaining variables fixed. Assuming that the global constraints of the optimization problem can be decomposed into the Cartesian product of the constraint sets of each block of variables, the resulting sequence of block-coordinate updates is guaranteed to converge to a stationary point [2].

In the case of NMF, the overall non-negativity constraints are in fact the Cartesian product of the non-negativity constraints on the individual variables. Hence, the NMF optimization problem can be tackled in a block-coordinate descent approach. The most elemental block coordinate descent approach to NMF uses \mathbf{A} and \mathbf{B} as coordinate block. The resulting optimization technique is sketched in Algorithm 1.

NMF methods which adopt this optimization technique are, e.g., the *Multiplicative Updates rule* [15], the *Active-Set-Like* method [12] or *Projected Gradient Descent* NMF [17]. However, these methods are *computationally expensive* and associated to a *slow convergence rate* [13]. In fact, they are

Algorithm 1 NMF block-coordinate descent approach.

- 1: **for** iterations (i) **do**
 - 2: $\mathbf{A}^{(i+1)} \leftarrow \underset{\mathbf{A}, \mathbf{A} \geq 0}{\operatorname{argmin}} J(\mathbf{A}^{(i)}, \mathbf{B}^{(i)} \mid \mathbf{X}) = \frac{1}{2} \|\mathbf{X} - \mathbf{A}^{(i)} \mathbf{B}^{(i)T}\|_F^2$ \triangleright \mathbf{B} fixed
 - 3: $\mathbf{B}^{(i+1)} \leftarrow \underset{\mathbf{B}, \mathbf{B} \geq 0}{\operatorname{argmin}} J(\mathbf{A}^{(i+1)}, \mathbf{B}^{(i)} \mid \mathbf{X}) = \frac{1}{2} \|\mathbf{X} - \mathbf{A}^{(i+1)} \mathbf{B}^{(i)T}\|_F^2$ \triangleright \mathbf{A} fixed
 - 4: **if** convergence criterion is reached **then** Stop iterations **end if**
 - 5: **end for**
-

characterized by large memory needs that scale with $\mathcal{O}(dn + dk + nk)$ and involve a large number of Floating Point Operations (FLOPS) per iterative update ($\sim \mathcal{O}(2dnk)$).

2.2 Hierarchical Optimization Methods

The Hierarchical Alternating Least Squares (HALS) method for NMF was originally proposed by [6, 4] as an improvement of the Alternating Least Squares (ALS) method [5]. It consists of a block-coordinate descent method with single component vectors as coordinate blocks. In this context, the cost function from equation (2) can be modified to define a set of cost functions:

$$J(\mathbf{a}_j, \mathbf{b}_j \mid \mathbf{X}_j) = \|\mathbf{X}_j - \mathbf{a}_j \mathbf{b}_j^T\|_F^2 \quad \forall j \in [1, \dots, k], \quad (3)$$

one for each component vector \mathbf{a}_j and \mathbf{b}_j such that $\mathbf{A} = [\mathbf{a}_1, \mathbf{a}_2, \dots, \mathbf{a}_k]$ and $\mathbf{B} = [\mathbf{b}_1, \mathbf{b}_2, \dots, \mathbf{b}_k]$ and where \mathbf{X}_j is:

$$\mathbf{X}_j = \mathbf{X} - \mathbf{A} \mathbf{B}^T + \mathbf{a}_j \mathbf{b}_j^T \quad \forall j \in [1, \dots, k], \quad (4)$$

where the computed expectation of \mathbf{X} , provided by the j^{th} components of \mathbf{A} and \mathbf{B} is added to the residual matrix. The global optimization problem based on equation (3) can be addressed by the set of iterative updates presented in Algorithm 2.

Algorithm 2 NMF Hierarchical Alternating Least Squares approach.

- 1: **for** iterations (i) **do**
 - 2: **for** components (j) **do**
 - 3: $\mathbf{a}_j^{(i+1)} \leftarrow \underset{\mathbf{a}_j, \mathbf{a}_j \geq 0}{\operatorname{argmin}} J(\mathbf{a}_j^{(i)}, \mathbf{b}_j^{(i)} \mid \mathbf{X}_j) = \frac{1}{2} \|\mathbf{X}_j - \mathbf{a}_j^{(i)} \mathbf{b}_j^{(i)T}\|_F^2$ \triangleright \mathbf{b}_j fixed
 - 4: $\mathbf{b}_j^{(i+1)} \leftarrow \underset{\mathbf{b}_j, \mathbf{b}_j \geq 0}{\operatorname{argmin}} J(\mathbf{a}_j^{(i+1)}, \mathbf{b}_j^{(i)} \mid \mathbf{X}_j) = \frac{1}{2} \|\mathbf{X}_j - \mathbf{a}_j^{(i+1)} \mathbf{b}_j^{(i)T}\|_F^2$ \triangleright \mathbf{a}_j fixed
 - 5: **end for**
 - 6: **if** convergence criterion is reached **then** Stop iterations **end if**
 - 7: **end for**
-

The HALS method provides alternating updates on a single component level which typically result in higher convergence rate and better data approximation compared to the methods introduced on Section 2.1 [13]. On the other hand, the iterative update rules of HALS are computationally more expensive if compared to the block coordinate descent based method, with a number of FLOPS per iteration $\sim \mathcal{O}(8dnk)$. This computational limit was partially overcome by the introduction of FastHALS [5], a more efficient update rule for HALS which scales as $\mathcal{O}(4dnk)$. However, a critical issue remains: For

large datasets the HALS algorithm still requires the entire data matrix \mathbf{X} to be held in memory in order to be fast. Hence the memory consumption still scales with $\mathcal{O}(dn + dk + nk)$.

3 Random Projection

Random projection is a dimensionality reduction technique for datapoints lying in a Euclidean space. It is commonly adopted to reduce the problem of managing and manipulating large datasets for techniques such as PCA, Singular Value Decomposition, Manifold Learning [24] and NMF [22, 3]. Its significance is mostly due to the *Johnson-Lindenstrauss lemma* which proves that random projections well preserve the pairwise Euclidean distances between datapoints [7]. For this exact same reason, NMF methods with random projection provide data approximation results almost as accurate as their standard uncompressed counterparts [22]. In this section we provide a general introduction to the random projections technique while the application of this method to the context of NMF will be discussed in section 3.1.

The random projections are characterized by a simple computational scheme. Let us define $r \in \mathbb{N}$ as the rank of the given data matrix $\mathbf{X} \in \mathbb{R}^{d \times n}$, with $r_{ov} \in \mathbb{N}$ as an oversampling parameter and $\mathbf{\Omega} \in \mathcal{N}(0, 1)^{n \times (r+r_{ov})}$ as a Gaussian random matrix whose entries are standard normal random variables. The structured random projection operation [22] can be defined as:

$$\hat{\mathbf{X}} = \mathbf{Q}^T \mathbf{X} \quad (5)$$

where $\mathbf{Q} := \mathbb{R}^{d \times n} \rightarrow \mathbb{R}^{(r+r_{ov}) \times n}$ is the random projection operator that maps the datapoints from the original dataspace onto the randomly selected subspace. The orthogonal matrix \mathbf{Q} is defined by the QR decomposition of the data transformation $P(\mathbf{X})$:

$$P(\mathbf{X}) = (\mathbf{X}\mathbf{X}^T)^w \mathbf{X}\mathbf{\Omega}, \quad (6)$$

where $w \in \mathbb{N}$ is the power iterations parameter [9]. For large input matrices \mathbf{X} , the singular vectors associated with small singular values will interfere with the calculation of the random projection matrix. Thanks to the factor $(\mathbf{X}\mathbf{X}^T)^w$ the decay rate of the singular power spectrum $\sigma_j(\mathbf{X})$ will be increased to:

$$\sigma_j((\mathbf{X}\mathbf{X}^T)^w \mathbf{X}) = \sigma_j(\mathbf{X})^{2w+1} \text{ with } j = 1, 2, 3, \dots \quad (7)$$

This preserves the singular vectors of \mathbf{X} while rendering the larger singular values more dominant for the definition of \mathbf{Q} . In the following section we will introduce the state of the art techniques which incorporate random projections into the block coordinate descent approach for NMF.

3.1 Random Projection and Semi-NMF

According to the definition of the operator \mathbf{Q} given in equation (5), random projection operators do not preserve the property of non-negativity of a non-negative dataset \mathbf{X} . For this reason, NMF techniques

with random projection are addressed in terms of two different objective functions which are defined in terms of the two non negative factor matrices \mathbf{A} and \mathbf{B} .

Let us define the two random projection matrices $\mathbf{L} \in \mathbb{R}^{d \times (r+r_{ov})}$ and $\mathbf{R} \in \mathbb{R}^{(r+r_{ov}) \times n}$ respectively from $P(\mathbf{X})$ and $P(\mathbf{X}^T)$ and assuming that $\min(d, n) \gg (r + r_{ov}) > k$. The NMF problem with random projection can be defined as the alternating optimization problem, as shown in Algorithm 3, where the optimization problems of line 2 and 3 are addressed in terms of the Semi-NMF method [8].

Algorithm 3 semi-NMF with random projection

- 1: **for** iterations (i) **do**
 - 2: $\mathbf{A}^{(i+1)} \leftarrow \underset{\mathbf{A}, \mathbf{A} \geq 0}{\operatorname{argmin}} J(\mathbf{A}^{(i)}, \mathbf{B}^{(i)} | \mathbf{X}\mathbf{R}^T) = \frac{1}{2} \|\mathbf{X}\mathbf{R}^T - \mathbf{A}^{(i)}\mathbf{B}^{(i)T}\mathbf{R}^T\|_F^2$ \triangleright \mathbf{B} fixed
 - 3: $\mathbf{B}^{(i+1)} \leftarrow \underset{\mathbf{B}, \mathbf{B} \geq 0}{\operatorname{argmin}} J(\mathbf{L}^T \mathbf{A}^{(i+1)}, \mathbf{B}^{(i)} | \mathbf{L}^T \mathbf{X}) = \frac{1}{2} \|\mathbf{L}^T \mathbf{X} - \mathbf{L}^T \mathbf{A}^{(i+1)}\mathbf{B}^{(i)T}\|_F^2$ \triangleright \mathbf{A} fixed
 - 4: **if** convergence criterion is reached **then** Stop iterations **end if**
 - 5: **end for**
-

According to Algorithm 3, only the currently updated and not projected factor matrix is assumed to be non-negative.

4 HALS with Random Projection

In this section we formally introduce two new NMF block coordinate descent approaches incorporating random projections, based on the HALS and FastHALS methods. According to the definition of \mathbf{L} and \mathbf{R} , given in section 3.1, Algorithm 4 shows how random projections can be included in the computational scheme described by Algorithm 2, where $\hat{\mathbf{X}} = \mathbf{L}^T \mathbf{X}$ and $\check{\mathbf{X}} = \mathbf{X}\mathbf{R}^T$ are the *left-* and *right-projected* datasets respectively, $\hat{\mathbf{A}} = \mathbf{L}^T \mathbf{A}$ and $\check{\mathbf{B}} = \mathbf{R}\mathbf{B}$ are the compressed factors with components $\hat{\mathbf{a}}_j = \mathbf{L}^T \mathbf{a}_j$ and $\check{\mathbf{b}}_j = \mathbf{R}\mathbf{b}_j$ and $\hat{\mathbf{X}}_j$ and $\check{\mathbf{X}}_j$ are defined as:

$$\begin{aligned} \hat{\mathbf{X}}_j &= \hat{\mathbf{X}} - \hat{\mathbf{A}}\mathbf{B}^T + \hat{\mathbf{a}}_j\mathbf{b}_j^T \\ \check{\mathbf{X}}_j &= \check{\mathbf{X}} - \mathbf{A}\check{\mathbf{B}}^T + \mathbf{a}_j\check{\mathbf{b}}_j^T. \end{aligned} \quad (8)$$

Algorithm 4 Hierarchical Alternating Least Squares with Random Projection

- 1: **for** iteration (i) **do**
 - 2: **for** components (j) **do**
 - 3: $\mathbf{a}_j^{(i+1)} \leftarrow \underset{\mathbf{a}_j, \mathbf{a}_j \geq 0}{\operatorname{argmin}} J(\mathbf{a}_j^{(i)}, \check{\mathbf{b}}_j^{(i)} | \check{\mathbf{X}}_j) = \frac{1}{2} \|\check{\mathbf{X}}_j - \mathbf{a}_j^{(i)}\check{\mathbf{b}}_j^{(i)T}\|_F^2$ \triangleright \mathbf{B} fixed
 - 4: $\mathbf{b}_j^{(i+1)} \leftarrow \underset{\mathbf{b}_j, \mathbf{b}_j \geq 0}{\operatorname{argmin}} J(\hat{\mathbf{a}}_j^{(i+1)}, \mathbf{b}_j^{(i)} | \hat{\mathbf{X}}_j) = \frac{1}{2} \|\hat{\mathbf{X}}_j - \hat{\mathbf{a}}_j^{(i+1)}\mathbf{b}_j^{(i)T}\|_F^2$ \triangleright \mathbf{A} fixed
 - 5: **end for**
 - 6: **if** convergence criterion is reached **then** Stop iterations **end if**
 - 7: **end for**
-

The explicit form of the iterative update rules in line 3 and 4 of Algorithm 4 can be found by computing the local gradient of the two cost functions $J(\mathbf{a}_j, \check{\mathbf{b}}_j | \check{\mathbf{X}}_j)$ and $J(\hat{\mathbf{a}}_j, \mathbf{b}_j | \hat{\mathbf{X}}_j)$ with respect

to the unknown factor vectors \mathbf{a}_j and \mathbf{b}_j as:

$$\frac{\partial J(\mathbf{a}_j, \check{\mathbf{b}}_j \mid \check{\mathbf{X}}_j)}{\partial \mathbf{a}_j} = (\mathbf{a}_j \check{\mathbf{b}}_j^T \check{\mathbf{b}}_j - \check{\mathbf{X}}_j \check{\mathbf{b}}_j), \quad (9)$$

$$\frac{\partial J(\hat{\mathbf{a}}_j, \mathbf{b}_j \mid \hat{\mathbf{X}}_j)}{\partial \mathbf{b}_j} = (\mathbf{b}_j \hat{\mathbf{a}}_j^T \hat{\mathbf{a}}_j - \hat{\mathbf{X}}_j^T \hat{\mathbf{a}}_j). \quad (10)$$

By equating the gradient components to zero, the iterative update scheme for the HALS-RP method follows directly from equation (9) and (10) as:

$$\mathbf{a}_j \leftarrow \left[\frac{\check{\mathbf{X}}_j \check{\mathbf{b}}_j}{\check{\mathbf{b}}_j^T \check{\mathbf{b}}_j} \right]_+, \quad \mathbf{b}_j \leftarrow \left[\frac{\hat{\mathbf{X}}_j^T \hat{\mathbf{a}}_j}{\hat{\mathbf{a}}_j^T \hat{\mathbf{a}}_j} \right]_+; \quad (11)$$

where the non-negativity of \mathbf{a}_j and \mathbf{b}_j is imposed after each iterative update by setting the negative values of the solution to zero.

According to the derivation of the FastHALS method presented in [6], we introduce an alternative and computationally more efficient update rule for the HALS-RP algorithm, named FastHALS-RP. This new method is defined by including the explicit expressions for $\hat{\mathbf{X}}$ and $\check{\mathbf{X}}$ from equation (8) in equations (11) as:

$$\begin{aligned} \mathbf{a}_j &\leftarrow \left[\mathbf{a}_j + \frac{\check{\mathbf{X}} \check{\mathbf{b}}_j - \mathbf{A} \check{\mathbf{B}}^T \check{\mathbf{b}}_j}{\check{\mathbf{b}}_j^T \check{\mathbf{b}}_j} \right]_+ = \left[\mathbf{a}_j + \frac{(\check{\mathbf{X}} \check{\mathbf{B}})_j - \mathbf{A} (\check{\mathbf{B}}^T \check{\mathbf{B}})_j}{(\check{\mathbf{B}}^T \check{\mathbf{B}})_{jj}} \right]_+, \\ \mathbf{b}_j &\leftarrow \left[\mathbf{b}_j + \frac{\hat{\mathbf{X}}^T \hat{\mathbf{a}}_j - \mathbf{B} \hat{\mathbf{A}}^T \hat{\mathbf{a}}_j}{\hat{\mathbf{a}}_j^T \hat{\mathbf{a}}_j} \right]_+ = \left[\mathbf{b}_j + \frac{(\hat{\mathbf{X}}^T \hat{\mathbf{A}})_j - \mathbf{B} (\hat{\mathbf{A}}^T \hat{\mathbf{A}})_j}{(\hat{\mathbf{A}}^T \hat{\mathbf{A}})_{jj}} \right]_+; \end{aligned} \quad (12)$$

where the normalization of the factor vectors is iteratively imposed with $\mathbf{a}_j = \mathbf{a}_j / \|\mathbf{a}_j\|_2$.

4.1 Sparsity and Smoothness constraints

In order to enforce the properties of smoothness and sparsity of the factor matrix \mathbf{B} , we introduce two additional penalty terms to the likelihood function presented in line 4 of Algorithm 4 as:

$$J(\hat{\mathbf{a}}_j, \mathbf{b}_j \mid \hat{\mathbf{X}}_j) = \frac{1}{2} \|\hat{\mathbf{X}}_j - \hat{\mathbf{a}}_j \mathbf{b}_j^T\|_F^2 + \alpha \|\mathbf{b}_j\|_1 + \frac{\beta}{2} \|\mathbf{b}_j\|_2^2, \quad (13)$$

where $\alpha \in \mathbb{R}_+$ and $\beta \in \mathbb{R}_+$ are the two parameters regulating the sparsity and smoothness levels of \mathbf{b}_j while $\|\cdot\|_1$ is the L_1 norm. Following the same derivation scheme presented in section 4, the HALS-RP update rules for \mathbf{a}_j and \mathbf{b}_j are:

$$\begin{aligned} \mathbf{a}_j &\leftarrow \left[\frac{\check{\mathbf{X}}_j \check{\mathbf{b}}_j}{\check{\mathbf{b}}_j^T \check{\mathbf{b}}_j} \right]_+, \\ \mathbf{b}_j &\leftarrow \frac{\left[\hat{\mathbf{X}}_j^T \hat{\mathbf{a}}_j - \alpha \mathbf{1}_n \right]_+}{\hat{\mathbf{a}}_j^T \hat{\mathbf{a}}_j + \beta}, \end{aligned} \quad (14)$$

where $\mathbb{1}_n$ denotes the vector made of all unitary entries with length n . Analogously, imposing the same constraints for the vector \mathbf{b}_j computed by the FastHALS-RP method, we get the following update rules:

$$\begin{aligned} \mathbf{a}_j &\leftarrow \left[\mathbf{a}_j + \frac{\mathbf{H}_j - \mathbf{A}\mathbf{G}_j}{\mathbf{G}_{jj}} \right]_+, \\ \mathbf{b}_j &\leftarrow \left[\frac{\mathbf{b}_j \hat{\mathbf{a}}_j^T \hat{\mathbf{a}}_j + \hat{\mathbf{X}}^T \hat{\mathbf{a}}_j - \mathbf{B}\hat{\mathbf{A}}^T \hat{\mathbf{a}}_j^T - \alpha \mathbb{1}_N}{\hat{\mathbf{a}}_j^T \hat{\mathbf{a}}_j + \beta} \right]_+ = \\ &\left[\frac{\mathbf{b}_j \mathbf{W}_{jj} + \mathbf{P}_j - \mathbf{B}\mathbf{W}_j - \alpha \mathbb{1}_N}{\mathbf{W}_{jj} + \beta} \right]_+, \end{aligned} \quad (15)$$

where $\mathbf{H} = \check{\mathbf{X}}\check{\mathbf{B}}$, $\mathbf{G} = \check{\mathbf{B}}^T\check{\mathbf{B}}$, $\mathbf{W} = \hat{\mathbf{A}}^T\hat{\mathbf{A}}$ and $\mathbf{P} = \hat{\mathbf{X}}^T\hat{\mathbf{A}}$.

4.2 Numerical Complexity and Memory Consumption

This section is aimed at evaluating the theoretical performance expectations of the different NMF algorithms presented in the previous sections. In particular, we are interested in assessing the improvements provided by random projections in terms of numerical complexity and memory consumption. Table 1 shows the performance comparison between the Multiplicative Update method (MU), the Hierarchical Least Squares method (HALS) and its more efficient implementation (FastHALS) with their variants using random projections i.e., MU-RP, HALS-RP and FastHALS-RP.

Method	Num. Complexity	Memory Consumption
MU	$\mathcal{O}(8dnk)$	$\mathcal{O}(dn + dk + nk)$
HALS	$\mathcal{O}(8dnk)$	$\mathcal{O}(dn + dk + nk)$
FastHALS	$\mathcal{O}(4dnk)$	$\mathcal{O}(dn + dk + nk)$
MU-RP	$\mathcal{O}(4dk(r + r_{ov}))$	$\mathcal{O}((2(r + r_{ov}) + k)(d + n))$
HALS-RP	$\mathcal{O}(4dnk(r + r_{ov}))$	$\mathcal{O}((2(r + r_{ov}) + k)(d + n))$
FastHALS-RP	$\mathcal{O}(2dk(r + r_{ov}))$	$\mathcal{O}((2(r + r_{ov}) + k)(d + n))$

Table 1: Numerical complexity and memory requirements for MU, HALS, FastHALS, MU-RP, HALS-RP and FastHALS NMF. All those values are computed under the assumption $d \gg (n, r, k)$.

According to Table 1, random projections reduces the numerical complexity associated to MU and FastHALS by a factor $2(r + r_{ov})/n$, while it increases by a factor $(r + r_{ov})/2$ for the HALS method. This discrepancy is a direct consequence of the methods' different computational arrangements. In particular, HALS-RP requires k different random projection steps within every iterative loop (one for each component \mathbf{a}_j and \mathbf{b}_j), leading to a strong increment of the numerical complexity in its iterative update step. In conclusion, random projections provide a reduction of the memory consumptions from $\mathcal{O}(dn + dk + nk)$ to $\mathcal{O}((2(r + r_{ov}) + k)(d + n))$ for all the presented NMF methods.

5 Experiments

This section is aimed at providing an overview of the numerical and computational properties of the NMF methods based on two real-world applications: a factorization of the *Olivetti faces dataset* and the *20 Newsgroups dataset* which represent dense and sparse data respectively. Our analysis is structured as follows: First, we investigate some of numerical and computational properties of the NMF methods, such as, convergence rate, reconstruction errors, numerical complexity and memory consumption. Second, we evaluate how the solutions computed by FastHALS and FastHALS-RP are influenced by different choices for the number of components k , the random projection parameter w and the sparsity and smoothness parameters, respectively α and β . For the assessment of the performance in the second step, we discuss measurable quantities, e.g. the final data approximation error and the sparsity level of \mathbf{B} . The measured quantities presented here were estimated as the median values over multiple independent runs of every algorithm to avoid biases in the results and to assess the stability of the methods against the initial random initialization of the factor matrices.

5.1 Olivetti Faces dataset

The Olivetti faces dataset [19] is composed of 400 images originally collected for the validation of face recognition algorithms [20]. Images, 64×64 pixels, are quantized to 256 gray scale levels and show the faces of 40 different subjects under varying light conditions and with different facial expressions (Figure 1).



Figure 1: Ten samples from the Olivetti faces dataset of images.

The first set of results presented in this section is based on runs over 500 iterations of the MU, MU-RP, HALS, HALS-RP, FastHALS and FastHALS-RP NMF algorithms applied to the Olivetti faces dataset. We choose the number of components $k = 20$ for all the NMF methods while we keep $r + r_{ov} = 25$ and $w = 4$ fixed for the MU-RP, HALS-RP and FastHALS-RP algorithms. Figure 2 shows the iterative evolution of the NMF data approximation error computed as $\frac{1}{2} \|\mathbf{X} - \mathbf{A}\mathbf{B}^T\|_F^2$. In

comparison with the other NMF methods, MU and MU-RP performs with higher reconstruction errors and smaller iterative convergence rates which can be interpreted as a direct consequence of the different computational granularity between the MU and the HALS based algorithms. Moreover, by considering the plot in Figure 2, it is not clear if MU and MU-RP will asymptotically converge to the same data approximation precision level of the other NMF methods. In table 2 we present the numerical complexity, memory consumption and average time per iteration values estimated for this application. According to these results, FastHALS-RP, together with MU-RP, outperform the other NMF methods in terms of average time per update. While FastHALS-RP has the lowest numerical complexity. In particular, FastHALS-RP allow for a numerical complexity level which is about the 40% lower with respect to the FastHALS method.

As already discussed in section 4.2, these results illustrate that in the HALS case, random projections come with additional computational cost. In fact, HALS-RP is computationally more expensive than HALS by more than one order of magnitude. Finally, the last column of table 2 shows that random projections provide a reduction of the NMF algorithms memory consumption of about the 80%.

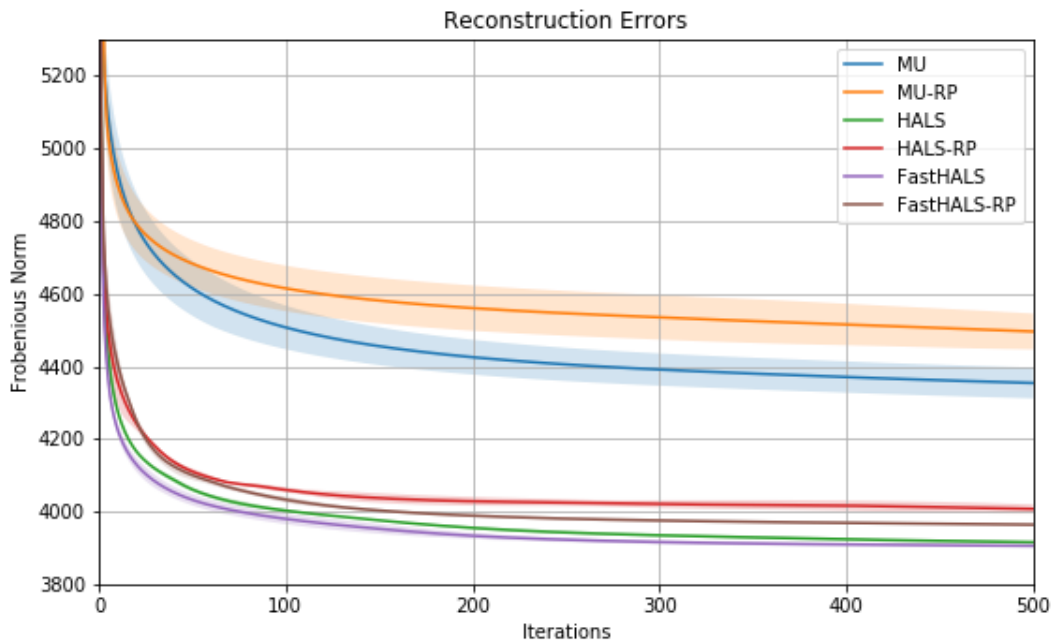


Figure 2: Evolution of the reconstruction errors over iterations for the MU, MU-RP, HALS, HALS-RP, FastHALS, FastHALS-RP NMF methods when applied to the Olivetti faces dataset.

The second set of assessments included in this section is aimed at estimating how different choices for the parameters k , w , α and β affect the approximation error of the FastHALS-RP method. Additionally, we investigate the effect on sparsity and smoothness properties of the computed factor \mathbf{B} .

Figure 3 compares the data reconstruction quality provided by FastHALS-RP and FastHALS which appear to be strongly dependent on the choice made for the parameters k and w . For the range of k values spanned by this analysis, $w = 3$ provides the most accurate results in terms of data approximation

Method	Complexity [10^6 flops]	Time per update [seconds]	Memory [10^4 floats]
MU	270	0.031	170
MU-RP	13	0.023	31
HALS	260	0.332	170
HALS-RP	3200	0.575	31
FastHALS	14	0.035	170
FastHALS-RP	8.6	0.023	31

Table 2: NMF methods numerical complexity, memory consumption and time per update estimated for the Olivetti faces applications.

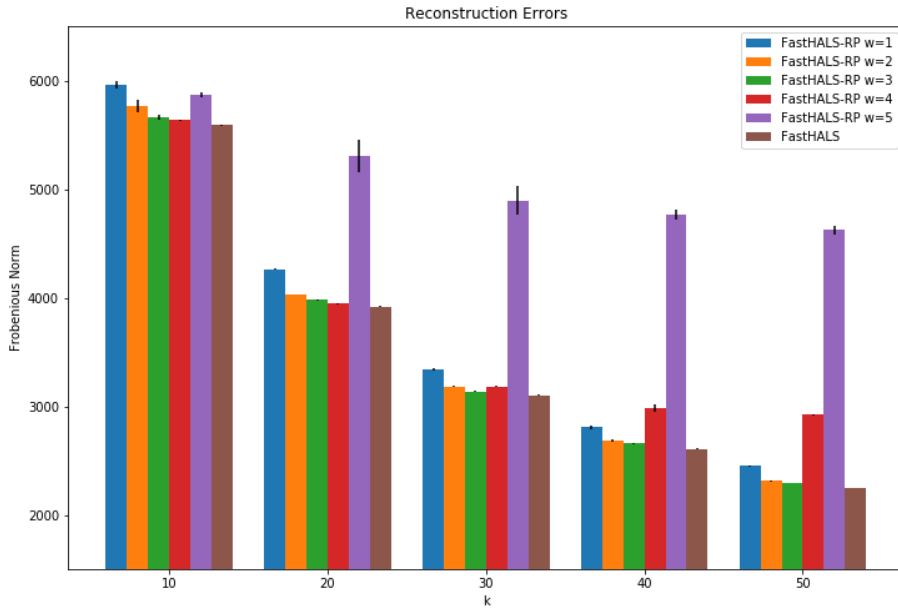


Figure 3: Comparison between the approximation errors provided by FastHALS and FastHALS-RP for $k = [10, 20, 30, 40, 50]$ and $w = [1, 2, 3, 4, 5]$.

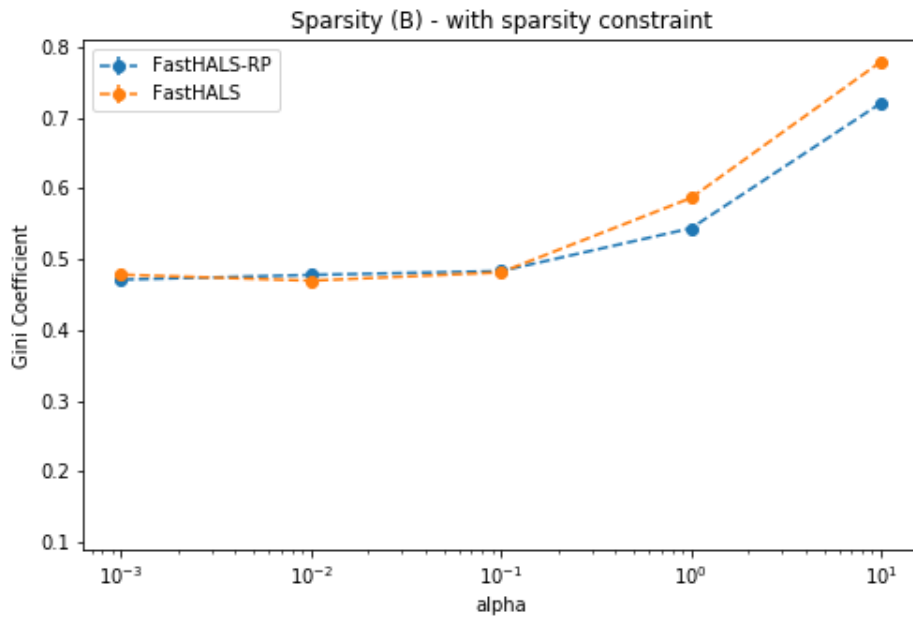


Figure 4: Gini coefficients of the \mathbf{B} matrix computed by FastHALS and FastHALS-RP with sparsity parameter $\alpha = [0.001, 0.01, 0.1, 1, 10]$, number of components $k = 20$ and random projection parameter $w = 3$.

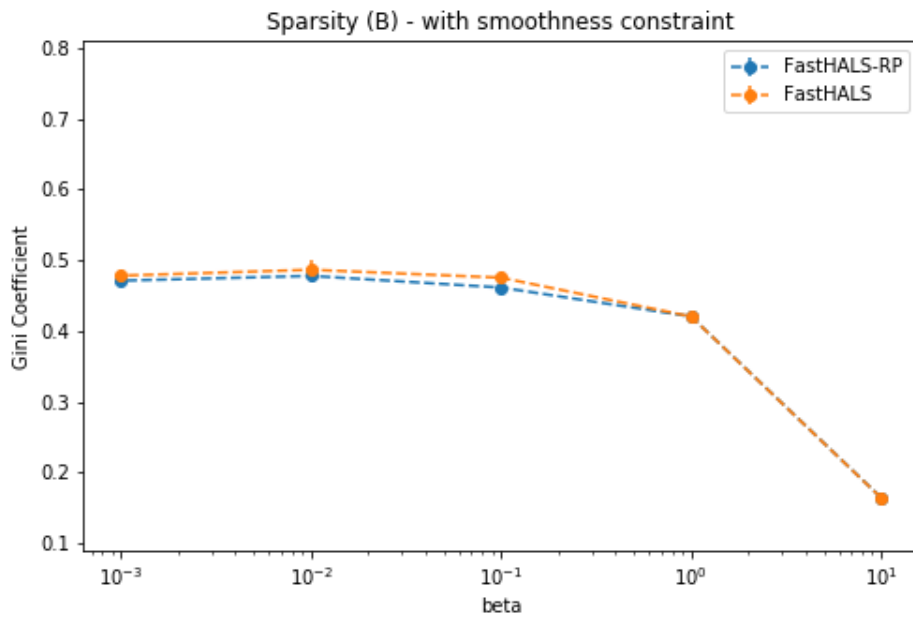


Figure 5: Gini coefficients of the \mathbf{B} matrix computed by FastHALS and FastHALS-RP with smoothness parameter $\beta = [0.001, 0.01, 0.1, 1, 10]$, number of components $k = 20$ and random projection parameter $w = 3$.

precision.

Figures 4 and 5 show how the sparsity level of the factor matrix \mathbf{B} computed by FastHALS-RP and FastHALS is influenced by the parameters α and β . The sparsity level of \mathbf{B} was estimated in terms of the Gini coefficient:

$$G = \frac{\sum_{i=1}^{n \cdot k} (2i - (n \cdot k) - 1) \mathbf{B}_i^S}{(n \cdot k) \sum_{i=1}^{n \cdot k} \mathbf{B}_i^S}, \quad (16)$$

where \mathbf{B}^S is the vector containing the values of the matrix \mathbf{B} sorted in ascending order. Figure 4 shows that the sparsity level of the factor matrix \mathbf{B} grows consistently with the parameter α . Moreover, for $\alpha < 0.1$ the two methods provide similar solution in terms of the Gini Coefficients profiles, while they start to deviate from each other for $\alpha \geq 0.1$ where FastHALS provides matrices \mathbf{B} with sparser values than FastHALS-RP. Figure 5 shows that for both FastHALS and FastHALS-RP, the sparsity level of \mathbf{B} decreases by increasing the value of the parameter β . In particular, for dense dataset the parameter β does not introduce any relative variation between the two considered sparsity profiles.

5.2 20 Newsgroups dataset

The 20 Newsgroups dataset [14] is a collection of approximately 20000 text documents, evenly partitioned over 20 different newsgroups classes. The analysis presented in this section is based on the application of the NMF methods on the frequency matrix associated with the 1000 most frequent words within the first 5000 samples. The resulting frequency matrix is sparse which provides a completely different numerical framework compared to the one provided by Olivetti faces dataset. Following the same structure as in section 5.1, we first focus on the reconstruction precision computed by 150 iterations of the NMF methods, with an arbitrary number of components $k = 60$ and with $r + r_{ov} = 72$ and $w = 9$ for the methods MU-RP, HALS-RP and FastHALS-RP.

Figure 6 shows that, also in the case of the 20 Newsgroup dataset, both MU and MU-RP are associated with a smaller convergence rate than the other NMF methods. Moreover, according to their iterative evolution profiles, these methods appear to be numerically more stable compared to the results presented in Figure 2 for the Olivetti faces dataset. Moreover, Figure 6 shows that NMF methods with random projections provide similar results to their standard counterparts in terms of data approximation error, with a few percent maximum deviation from the best performing algorithm FastHALS.

From table 3 we can see that the theoretical value of the numerical complexity for the FastHALS-RP iterations is one order of magnitude lower than the one of its unprojected counterpart FastHALS. This is reflected by an averaged time per update 1.5 times lower. Moreover, memory consumption levels are reduced by a factor ~ 3.5 in this application case when using random projections.

In analogy with 5.1, we present a comparison between the results provided by FastHALS-RP and FastHALS to assess how the reconstruction errors are affected by different choices of the number of components k and random projection parameter w . For this analysis we are considering $k = [50, 60, 70, 80, 90]$ and $w = [1, 3, 5, 7, 9, 11]$. Figure 7 shows that for this application the optimal choice is $w = 11$, independently of the the number of components k . The discrepancy between this

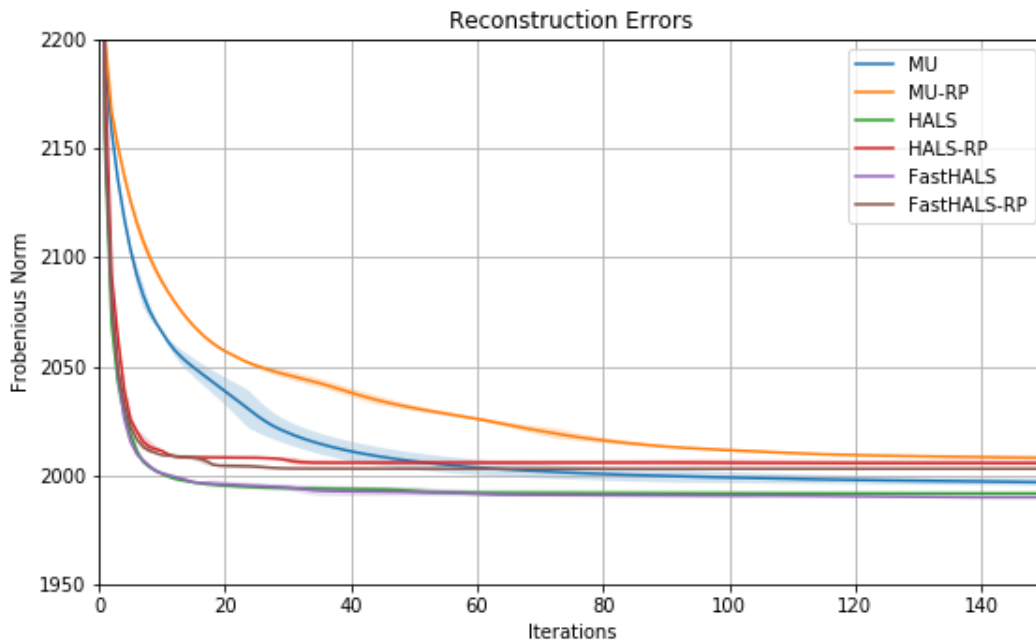


Figure 6: Evolution of the reconstruction error over iterations for the MU, MU-RP, HALS, HALS-RP, FastHALS, FastHALS-RP NMF methods when applied to the 20 Newsgroup dataset.

Method	Complexity [10^6 flops]	Time per update [seconds]	Memory [10^5 float]
MU	2400	0.068	53
MU-RP	150	0.048	12
HALS	2400	2.678	53
HALS-RP	430000	4.775	12
FastHALS	1300	0.069	53
FastHALS-RP	98	0.047	12

Table 3: Numerical complexity, average time per update and memory consumption for the NMF of the 20 Newsgroups dataset.

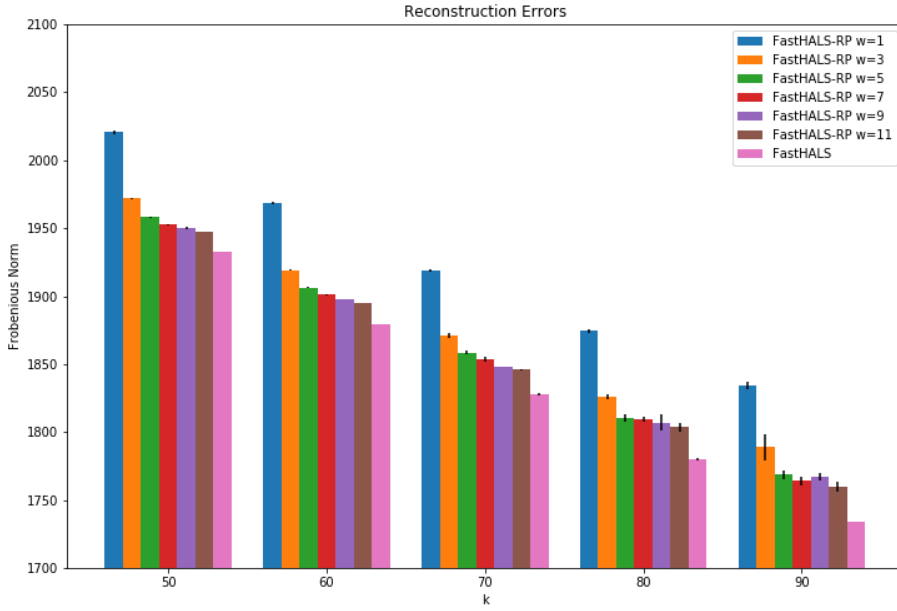


Figure 7: Comparison of the median reconstruction errors resulting from the FastHALS and FastHALS-RP methods when considering $k = [50, 60, 70, 80, 90]$ and $w = [1, 3, 5, 7, 9, 11]$.

value for w and the one found for the Olivetti faces dataset is due to the different decay rates p of the singular value spectra $\sigma_j(X)^{-p}$ of the two dataset. In particular, for the 20 Newsgroup dataset $p_{20_Newsgroups} \sim 0.0012$ while for the Olivetti faces dataset $p_{Olivetti} \sim 0.0053$. With the ratio $\sim 20\%$ between $p_{20_Newsgroups}$ and $p_{Olivetti}$, for the 20 Newsgroups dataset a higher value of w is required to *regularize* the distortion effects due to small singular values for the definition of the random projection operators L and R .

Finally, we assess how the sparsity level of the factor matrix \mathbf{B} changes for different choices of the parameters α and β when keeping $k = 60$ and $w = 9$.

From Figure 8 and 9, the sparsity and smoothness properties of \mathbf{B} show coherent behaviors to the one presented for the Olivetti Faces dataset. In particular, the Gini coefficients profiles for both the solutions provided by FastHALS and FastHALS-RP grow as function of α and decrease for larger values of β .

Figure 8 shows that, for the same set of values for α , FastHALS-RP provides solutions which are generally sparser than FastHALS. Moreover, the two methods seem to react differently to different choice of the parameter β , as shown in Figure 9. In particular, over the same range of β values we assessed that FastHALS-RP provides a stronger variations in the profile of Gini coefficients than FastHALS.

In conclusion, both Figure 8 and 9 shows that for a sparse dataset and without imposing any sparsity and smoothness constraint, the solutions for \mathbf{B} provided by FastHALS-RP are generally sparser than the

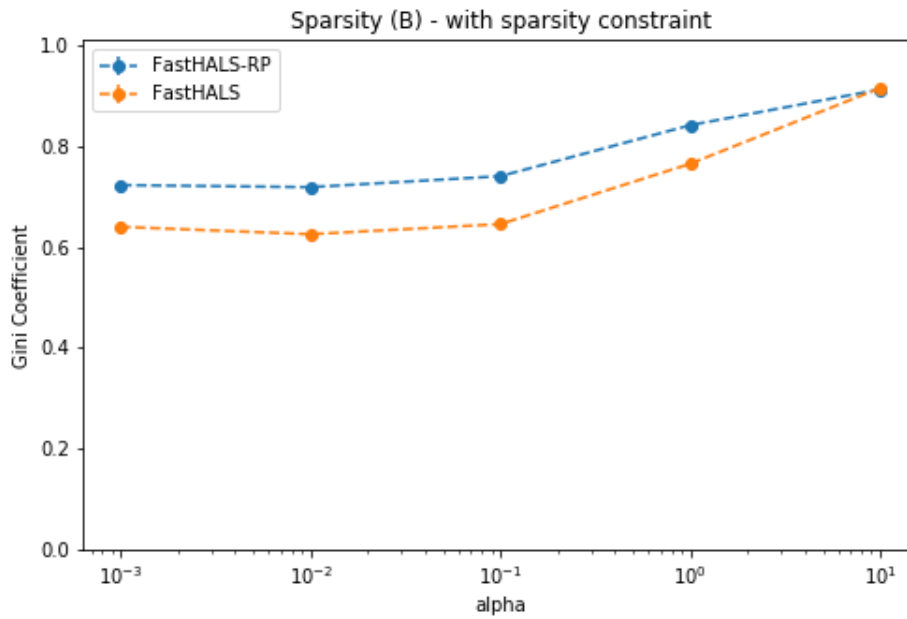


Figure 8: Gini coefficients of the \mathbf{B} matrix computed by FastHALS and FastHALS-RP with sparsity parameter $\alpha = [0.001, 0.01, 0.1, 1, 10]$, number of components $k = 60$ and random projection parameter $w = 9$.

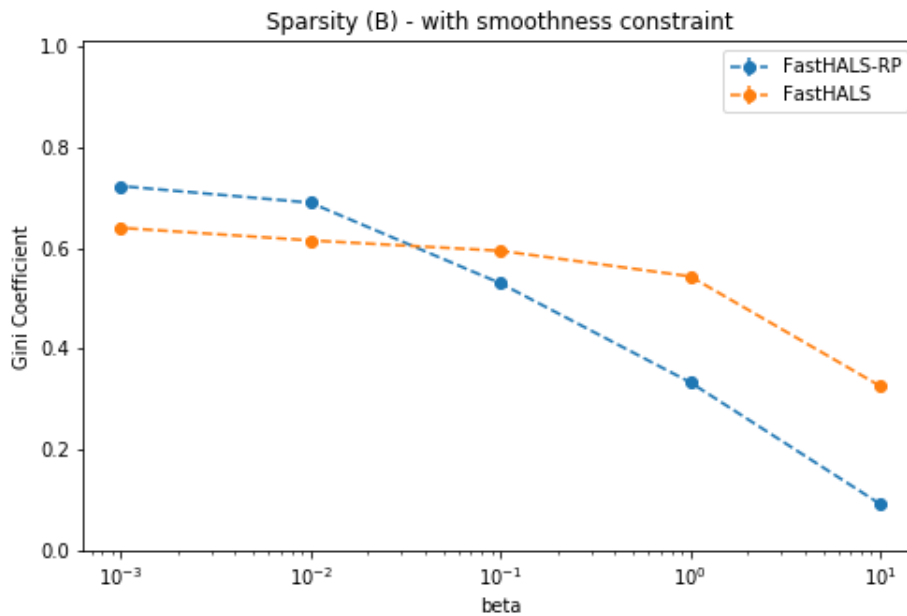


Figure 9: Gini coefficients of the \mathbf{B} matrix computed by FastHALS and FastHALS-RP with smoothness parameter $\beta = [0.001, 0.01, 0.1, 1, 10]$, number of components $k = 60$ and random projection parameter $w = 9$.

FastHALS ones. All those properties are a direct consequence of the application of Random Projections on a sparse dataset.

6 Conclusion

This paper was aimed at proposing FastHALS-RP, a novel NMF method capable of combining the fastest existing NMF algorithm FastHALS with a data dimensionality reduction scheme based on Random Projections. Our new algorithm outperforms the state of the art NMF methods both in computational efficiency and memory consumption.

With an appropriate choice of the parameters k and w , the desired number of components and the random projection power iteration parameter respectively, it has been shown that FastHALS-RP provides results with a data approximation precision level very close to the standard FastHALS method. In particular, we showed that the optimal choice for the parameter w strongly depends on the decay rate of the singular value spectrum of the data.

We showed that sparsity and smoothness constraints on the factor matrix \mathbf{B} can easily be introduced into the FastHALS-RP optimization problem. The conclusion of our analysis focused on assessing how the sparsity properties of the factor matrix \mathbf{B} , computed by FastHALS and FastHALS-RP, are influenced by different choices of α and β , the sparsity and smoothness coefficients in the likelihood function respectively. We found that for dense datasets and in absence of any sparsity and smoothness constraints for \mathbf{B} , FastHALS and FastHALS-RP provide solutions with similar sparsity property, while for sparse dataset, FastHALS-RP provides sparser solutions. For this reason, the effect of the two parameters α and β is different in the two scenarios and needs to be properly evaluated from case to case.

Some theoretical aspects regarding the optimal choice of the parameters w , $r + r_{ov}$, α and β still need to be investigated as well as the global convergence property of the algorithm.

While we could substantially reduce the memory footprint and speed up computation compared to existing methods, our algorithm still relies on being computed on a single node. A next step towards large-scale applications on distributed systems could now be to extend our algorithm with the map-reduce scheme proposed by [25]. We expect that such an approach will profit twice from our algorithm since we will not only see a speed-up on all nodes individually, but, in addition, the data transfer between nodes will be reduced which will lead to an additional speed-up.

We implemented the proposed method in Python and the source code will soon be publicly available.

Acknowledgements

Our work was supported by the two SNF Synergia Grant (*EUCLID: high-precision cosmology in the dark sector*). We Would like to thank Martin Melchior, André Csillaghy and Roman Bolzern for helping and providing comments that greatly improved the quality of this manuscript.

References

- [1] Olivier Berné, A Helens, P Pilleri, and C Joblin. Non-negative matrix factorization pansharpener of hyperspectral data: An application to mid-infrared astronomy. In *Hyperspectral Image and Signal Processing: Evolution in Remote Sensing (WHISPERS), 2010 2nd Workshop on*, pages 1–4. IEEE, 2010.
- [2] Dimitri P Bertsekas, Dimitri P Bertsekas, Dimitri P Bertsekas, and Dimitri P Bertsekas. *Dynamic programming and optimal control*, volume 1. Athena Scientific Belmont, MA, 1995.
- [3] Ella Bingham and Heikki Mannila. Random projection in dimensionality reduction: applications to image and text data. In *Proceedings of the seventh ACM SIGKDD international conference on Knowledge discovery and data mining*, pages 245–250. ACM, 2001.
- [4] Andrzej Cichocki and PHAN Anh-Huy. Fast local algorithms for large scale nonnegative matrix and tensor factorizations. *IEICE transactions on fundamentals of electronics, communications and computer sciences*, 92(3):708–721, 2009.
- [5] Andrzej Cichocki and Rafal Zdunek. Regularized alternating least squares algorithms for non-negative matrix/tensor factorization. *Advances in Neural Networks–ISNN 2007*, pages 793–802, 2007.
- [6] Andrzej Cichocki, Rafal Zdunek, and Shun-ichi Amari. Hierarchical als algorithms for nonnegative matrix and 3d tensor factorization. In *International Conference on Independent Component Analysis and Signal Separation*, pages 169–176. Springer, 2007.
- [7] Sanjoy Dasgupta and Anupam Gupta. An elementary proof of a theorem of johnson and lindenstrauss. *Random Structures & Algorithms*, 22(1):60–65, 2003.
- [8] Chris HQ Ding, Tao Li, and Michael I Jordan. Convex and semi-nonnegative matrix factorizations. *IEEE transactions on pattern analysis and machine intelligence*, 32(1):45–55, 2010.
- [9] Nathan Halko, Per-Gunnar Martinsson, and Joel A Tropp. Finding structure with randomness: Probabilistic algorithms for constructing approximate matrix decompositions. *SIAM review*, 53(2):217–288, 2011.
- [10] Aapo Hyvärinen and Erkki Oja. Independent component analysis: algorithms and applications. *Neural networks*, 13(4):411–430, 2000.
- [11] Ramakrishnan Kannan, Grey Ballard, and Haesun Park. A high-performance parallel algorithm for nonnegative matrix factorization. In *Proceedings of the 21st ACM SIGPLAN Symposium on Principles and Practice of Parallel Programming*, page 9. ACM, 2016.

- [12] Hyunsoo Kim and Haesun Park. Nonnegative matrix factorization based on alternating nonnegativity constrained least squares and active set method. *SIAM journal on matrix analysis and applications*, 30(2):713–730, 2008.
- [13] Jingu Kim, Yunlong He, and Haesun Park. Algorithms for nonnegative matrix and tensor factorizations: A unified view based on block coordinate descent framework. *Journal of Global Optimization*, 58(2):285–319, 2014.
- [14] Ken Lang. Newsweeder: Learning to filter netnews. In *Proceedings of the 12th international conference on machine learning*, pages 331–339, 1995.
- [15] Daniel D Lee and H Sebastian Seung. Learning the parts of objects by non-negative matrix factorization. *Nature*, 401(6755):788–791, 1999.
- [16] Daniel D Lee and H Sebastian Seung. Algorithms for non-negative matrix factorization. In *Advances in neural information processing systems*, pages 556–562, 2001.
- [17] Chih-Jen Lin. Projected gradient methods for nonnegative matrix factorization. *Neural computation*, 19(10):2756–2779, 2007.
- [18] Ryuichi Maruyama, Kazuma Maeda, Hajime Moroda, Ichiro Kato, Masashi Inoue, Hiroyoshi Miyakawa, and Toru Aonishi. Detecting cells using non-negative matrix factorization on calcium imaging data. *Neural Networks*, 55:11–19, 2014.
- [19] Olivetti Olivetti. Oracle research laboratory face database of faces.
- [20] Ferdinando Silvestro Samaria. *Face recognition using hidden Markov models*. PhD thesis, University of Cambridge, 1994.
- [21] Fariar Shahnaz, Michael W Berry, V Paul Pauca, and Robert J Plemmons. Document clustering using nonnegative matrix factorization. *Information Processing & Management*, 42(2):373–386, 2006.
- [22] Mariano Tepper and Guillermo Sapiro. Compressed nonnegative matrix factorization is fast and accurate. *IEEE Transactions on Signal Processing*, 64(9):2269–2283, 2016.
- [23] Santosh S Vempala. *The random projection method*, volume 65. American Mathematical Soc., 2005.
- [24] Fei Wang and Ping Li. Efficient nonnegative matrix factorization with random projections. In *Proceedings of the 2010 SIAM International Conference on Data Mining*, pages 281–292. SIAM, 2010.
- [25] Hsiang-Fu Yu, Cho-Jui Hsieh, Si Si, and Inderjit S Dhillon. Parallel matrix factorization for recommender systems. *Knowledge and Information Systems*, 41(3):793–819, 2014.

- [26] Le Zhang, Yu Yu, and Pengjie Zhang. Non-negative matrix factorization for self-calibration of photometric redshift scatter in weak lensing surveys. *arXiv preprint arXiv:1612.04042*, 2016.
- [27] Sheng Zhang, Weihong Wang, James Ford, and Fillia Makedon. Learning from incomplete ratings using non-negative matrix factorization. In *Proceedings of the 2006 SIAM International Conference on Data Mining*, pages 549–553. SIAM, 2006.